ELSEVIER

Inorganica Chimica Acta 226 (1994) 251–258

Inorganica Chimica Acta

The construction of molecular systems capable of photoinduced multielectron charge transfer: a photochemical analysis of the reactivity of $[(CN)_5Fe^{II}–(CN)–Pt^{IV}(L)_4–(NC)–Fe^{II}(CN)_5]^{4-}$ ($L = NH_3$, ethylenediamine)

Ying Wu, Carolyn Cohran, Andrew B. Bocarsly *

Department of Chemistry, Frick Laboratory, Princeton University, Princeton, NJ 08544-1009, USA

Received 21 March 1994

Abstract

The title trinuclear complexes are synthesized by the redox reaction of $[Fe(CN)_6]^{3-}$ and $[PtL_4]^{2+}$ (**A**: $L = NH_3$; **B**: L = 1/2 ethylenediamine). Both of these complexes exhibit an intervalence charge transfer (IT) band in the visible region of the optical spectrum. The energy of this transition is strongly dependent on temperature, as well as solvent. The energy of the IT band shifts by -17.3 ± 1.1 and -14.4 ± 0.7 cm^{-1}/K for **A** and **B**, respectively, within the temperature range of 0–45 °C. This shift is attributed to the temperature dependent redox potential of the $[Fe(CN)_6]^{4-/3-}$ moiety. The solvent dependence of the IT energy correlates with the electron-accepting ability of the solvent, and thus, the degree of H bonding between the solvent and the cyanide lone pairs. The nature of the solvent also affects the photodissociation quantum yield. This effect is reported in detail for **A** in a DMSO/water solvent mixture. The results can be interpreted using the Marcus–Hush charge transfer theory, which proves to be applicable to these systems capable of multielectron charge transfer.

Keywords: Photoinduced electron transfer; Iron complexes; Platinum complexes; Cyano complexes

1. Introduction

The practical conversion of optical energy to chemical energy via a redox type mechanism requires the ability to transfer more than one electron upon photoexcitation. Although this can be done electrochemically using a semiconducting electrode, there are very few molecular systems available which provide for this type of reactivity. This is true inspite of the successes, both theoretical and experimental, in developing an understanding of molecular based one-electron charge transfer processes. Because of the high degree of success in this latter area one strategy which has been suggested is the development of macromolecules containing a series of electronically linked chromophores [1]. In this case, the absorption of several photons by linked chromophoric units, leads to the production of multiple electrons. In contrast to this approach, systems might be designed which generate more than one electron upon absorption of one photon, a so called photoinduced multielectron charge transfer process. However, very few systems having this property have been identified to date, thus, it is difficult to identify the molecular electronic features which are essential for the observation of this type of reactivity.

Previously, we put forward a photoinduced multielectron charge transfer scheme which takes advantage of the high stability which platinum coordination complexes display for the II and IV oxidation states, and the high instability of such complexes toward the Pt(III) state [2]. Additionally, the complexes of interest must contain a chromophoric unit which can be utilized to activate the charge transfer process. If a potential solar energy conversion scheme is to be considered, the chromophore needs to absorb visible irradiation. The desired charge transfer transition must shift the platinum complex from one of its two stable oxidation states to the III state. Once this occurs a rapid follow up thermal, reaction back to one of the stable oxidation states is expected. This latter reaction will either regenerate the initial oxidation state leading to no net chemistry, or produce an oxidation state which varies by two electrons from the reactant. Because of the instability of Pt(III) the observation of a long lived one-electron product

* Corresponding author.

0020-1693/94/$07.00 © 1994 Elsevier Science S.A. All rights reserved
SSDI 0020-1693(94)04093-B

is precluded. That is, the system is primed to produce only multielectron products.

We initially reduced this reaction hypothesis to practice by synthesizing the supramolecular complexes: $\{L(CN)_4M^{II}(CN)[Pt^{IV}(NH_3)_4](NC)M^{II}(CN)_4L\}^{4-}$ (where M = Fe, Ru, or Os and L = CN^- or a σ-donor ligand) [3,4]. These compounds were found to exhibit an intense lowest energy transition that shifted energy linearly with the change in the redox potential of the 'M(CN)$_5$L' moiety brought about by variations in M and L. In addition, this band was found to disappear upon oxidation of M(II) to M(III). Based on these observations the lowest energy optical absorption band was assigned to an M(II) → Pt(IV) intervalent (IT) charge transfer band. When dissolved in aqueous solution, the iron analog was found to provide the desired two electron photoinduced charge transfer upon irradiation into the IT band [3] (Eq. (1)).

$$\{L(CN)_4Fe^{II}(CN)[Pt^{IV}(NH_3)_4](NC)Fe^{II}(CN)_4L\}^{4-} \xrightarrow{h\nu} [Pt^{II}(NH_3)_4]^{2+} + 2[Fe^{III}(CN)_5L]^{3-} \quad (1)$$

However, complexes where M = Ru or Os were found to be photoinert. Photochemical reactivity in these complexes could be induced by adding cosolvents such as DMSO which shift the M redox potential by destroying the hydrogen bonding network between water and the cyanide lone pairs [4,5].

The observed sensitivity of the photoinduced charge transfer to the M redox potential suggests that the observed chemistry can be described using a Marcus–Hush model in which the three intimate redox sites, {M(II)/Pt(IV)/M(II)}, are represented by three overlapping parabolas as shown in Fig. 1. Utilizing the nomenclature provided in Fig. 1, it is postulated that the observed net two-electron charge transfer involves optical excitation from A to F, followed by relaxation to C giving a highly reactive Pt(III) intermediate. This is then followed by a thermal electron transfer to yield the products (C → D → E). A thermal process from C back to A (C → B → A) is also accessible. As noted above the only long lived products are A and E, C is never obtained as a stable species. Thus, only net two-electron transfer are observed based on product analysis.

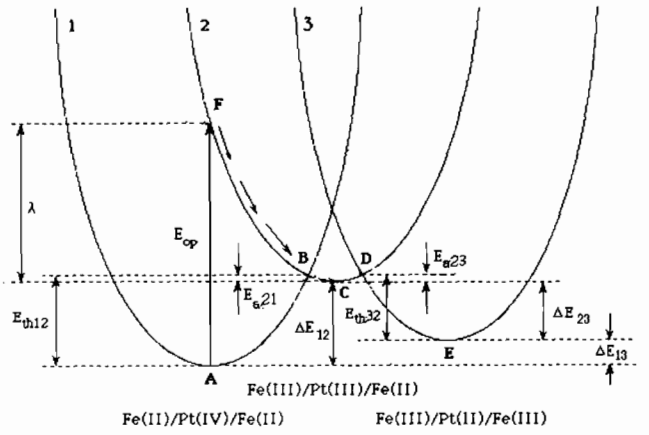

Fig. 1. Potential energy surfaces for Fe–Pt–Fe trinuclear complexes and related species.

In the current presentation, we seek to further test the proposed multielectron charge transfer model as well as to develop a more detailed understanding of the potential energy surfaces proposed in Fig. 1. To this end, complex **B**, the ethylenediamine substituted analog of the original complex (with M = Fe) has been synthesized. This complex not only dissolves in aqueous solutions like the parent compound, but a variety of neat organic solvents; thereby, allowing for an unambiguous analysis of the solvent dependence on the photophysics and photochemistry of the IT transition of interest. In addition a careful photophysical and ground state electrochemical evaluation of the parent complex (**A**) as a function of temperature and mixed DMSO/H_2O solvent has been executed. These latter studies are aimed at probing the energetics and dynamics of the charge transfer processes which traverse the ground state potential energy surface.

2. Experimental

2.1. Materials and instrumentation

Potassium ferricyanide ($K_3Fe(CN)_6$) and bis(ethylenediamine)platinum(II) chloride ($[Pt(en)_2]Cl_2$) were obtained from Fisher Scientific and Aldrich, respectively, and were used without further purification. Dowex-50 W cation exchange resin from Sigma was packed into a 1 × 30 cm column for sample purification. The column was washed with de-ionized water and NaCl solution before use, and the samples were eluted with water.

Room temperature UV–Vis spectra of the complexes were recorded on an HP 8450A diode-array spectrophotometer, and temperature dependent UV–Vis spectra were obtained on an HP 8542A diode array spectrophotometer equipped with a Fisher Scientific model 910 Isotemp refrigerated circulator to keep the cell holder at a constant temperature. IR spectra were obtained from KBr pellets in the mid-IR range on a Nicolet model 730 FTIR spectrophotometer.

A Coherent Innova 70 argon ion laser operating at 488 nm was used for photochemical measurements. Solutions of exactly 1.00 ml in volume were irradiated for 60 s at a time, and the disappearance of the trinuclear complex and the appearance of ferricyanide were monitored by recording the absorbance of the solutions at characteristic wavelengths immediately before and after irradiation. Irradiation intensity was monitored using a Newport Research model 815 power meter. Quantum yields were calculated in terms of the moles of ferricyanide generated per mole of photons absorbed.

All electrochemical studies were performed on a Princeton Applied Research 273 potentiostat interfaced to a NEC PowerMate computer. A standard one-compartment, three-electrode cell was employed using a Pt working electrode, a large Pt foil counter electrode, and an SCE reference electrode. Sodium nitrate, 1.0 M in concentration, was used as electrolyte. In the temperature dependent electrochemistry studies, a remote junction was used to thermally isolate the reference electrode at room temperature, while the solution temperature was varied. All uncertainties are based on the observed standard deviations of the data sets.

2.2. Preparation of complexes

The complex $[(CN)_5Fe–CN–Pt(en)_2–NC–Fe(CN)_5]^{4-}$ (**B**) was prepared according to the method reported for preparing $[(CN)_5Fe–CN–Pt(NH_3)_4–NC–Fe(CN)_5]^{4-}$ (**A**) [3]. The corresponding chemical equation is shown in Eq. (2).

$$2[Fe(CN)_6]^{3-} + [Pt(en)_2]^{2+} \longrightarrow [(CN)_5Fe–CN–Pt(en)_2–NC–Fe(CN)_5]^{4-} \quad (2)$$

Aqueous solutions of $K_3Fe(CN)_6$ (0.10 M) and $[Pt(en)_2]Cl_2$ (0.10 M), in 2:1.2 mole ratio, were mixed at room temperature. The reaction mixture turned dark red within 5 min, and it was allowed to stand in the dark for at least 1 h before it was passed through a Dowex 50W cation exchange column preloaded with Na^+ ions. The solid was isolated either by slow evaporation of water or by precipitation with careful addition of acetone followed by filtration. The stoichiometry of the reactants was determined by the Job method [6], in which the optical absorptivity at 472 nm was monitored as a function of the ratio of ferricyanide to Pt complex (Fig. 2), yielding a 2:1 ratio of Fe:Pt. The complex was characterized by UV–Vis spectroscopy ($\lambda_{max} = 434$ nm), IR spectroscopy (ν(bridging CN) = 2113 cm^{-1}, ν(terminal CN) = 2050 cm^{-1}), and cyclic voltammetry

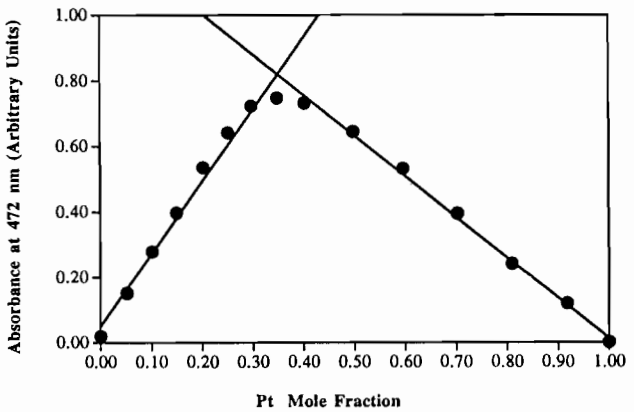

Fig. 2. Job plot depicting the 2:1 Fe/Pt ratio for complex **B** in aqueous solution with absorbance monitored at 472 nm.

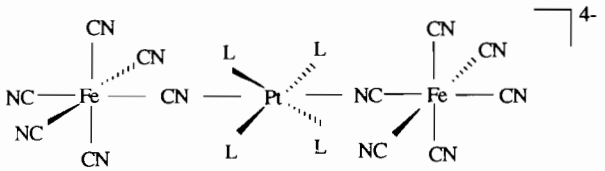

Fig. 3. Structural representation of the trinuclear complexes $[(NC)_5–Fe–CN–PtL_4–NC–Fe(CN)_5]^{4-}$, where L = NH_3 or 1/2(ethylenediamine).

($E_{1/2} = 0.56$ V versus SCE). A schematic representation of the trinuclear complex is shown in Fig. 3.

3. Results and discussion

3.1. Solvent-dependent intervalence charge transfer

Preliminary studies on the solvent dependence of the charge transfer energy were carried out using the sodium salt of complex **B**. A list of solvents capable of solvating complex **B** can be found in Table 1, along with their acceptor numbers (AN), and dielectric constants (ϵ). The absorption maxima are also listed. In order for the compound to dissolve, a large dielectric constant is required of the solvent to support the substantial charge (formally −4) on the complex. The lower limit appears to be methanol, which has a dielectric constant of 32.6.

Once dissolved, the complex exhibits a solvent-dependent IT band energy, presumably due to the difference in the solvent's donor–acceptor ability. In all solvents tested, except water, two absorption bands were observed. The higher energy one centers around 420 nm, and does not shift substantially with solvent. This band is assigned to the LMCT band of ferricyanide

Table 1
The energy of the intervalence charge transfer band for complex **B** in different solvents. The acceptor numbers (AN) and dielectric constants (ϵ) of the respective solvents are also listed [7]

Solvent	LMCT[a] (nm)	IT (nm)	AN	ϵ
N,*N*-Dimethylformamide (DMF)	424	570	16	36.7
Dimethyl sulfoxide (DMSO)	422	560	19.3	46.7
Formamide	422	522	39.8	109.5
Methanol (CH_3OH)	420	486	41.3	32.6
Ethylene glycol	424	476	42.1[b]	37.0
Glycerol	424	462	44.2[b]	42.5
Deuterium oxide (D_2O)		442	54.0[b]	78.25
Water (H_2O)		436	54.8	78.5

[a]Fe(II) → CN–π^* for ferricyanide formed from the decomposition of the complex.

[b]These acceptor numbers are calculated from Reichardt's polarity parameter $E_T(30)$ [8] according to the correlation developed by Kriegsmann [9].

which forms via the decomposition of the trinuclear complex, the reverse of Eq. (2). The lower energy band is assigned to the IT band of complex **B**, and shows strong solvatochromic behavior as shown in Table 1.

A quantitative correlation between the intervalence charge transfer energy and the electron-accepting ability of the solvents was investigated based on Gutmann's semiquantitative acceptor number (AN) scale [10]. A plot of IT band energy versus AN is shown in Fig. 4. With the exception of formamide, a linear relationship is observed between the IT energy and the acceptor number. We associate increased AN for the solvents selected with an improved ability to hydrogen bond to the cyanide lone pair. This correlation is consistent with Gutmann's prior observations on shifts in the $[Fe(CN)_6]^{4-/3-}$ redox potential with solvent [11]. Cyanide–solvent hydrogen bonding is expected to stabilize the CN–π^* orbital, giving rise to a lower-energy t_{2g} molecular orbital set in ferrocyanide. As a result, the redox potential difference, ΔE, and consequently the energy of the optical transition, E_{op}, becomes larger (see Eq. (6)). This relationship is best captured by comparing the effects of a D_2O to H_2O solvent. In this case, the only difference in the solvation interaction is expected to be the H versus D accepting behavior of the associated hydrogen bond (due to the change in the zero point energy of these two species). Therefore, for all solvents with the exception of formamide, the observed solvatochromic behavior can be understood in terms of a shift in the free energy of the charge transfer reaction and a relatively invariant solvent reorganization energy. On the other hand, formamide has an unusually large dielectric constant which evidently is reflected in the value of the reorganization energy, λ, when compared to the other solvents employed. Thus, the energy of the IT band in this solvent is apparently governed by both the effects of hydrogen bonding on the charge transfer free energy and the outer sphere reorganization energy. This latter term moves the IT band off the linear plot established by the other solvents.

In solvents such as DMF and DMSO, the hydrogen bonding interaction with cyanide is almost non-existent, and the IT band energy is very low. In these cases, $E_R(Fe^{III/II})$ approaches $E_R(Pt^{IV/II})$, leading to a large amount of decomposition of the trinuclear complex as illustrated in Eq. (3).

$$Fe^{II}\text{–}Pt^{IV}\text{–}Fe^{II} \rightleftharpoons 2Fe^{III} + Pt^{II} \quad (3)$$

When the solvent's electron-accepting ability is large, the interaction with the lone-pair on the cyanide nitrogen is stronger for the reduced species than the oxidized species, therefore, Fe^{II} is favored and the equilibrium lies to the left. This is the case for glycerol, glycol, water and deuterium oxide. Otherwise, the Fe^{III} species is favored and the equilibrium lies to the right. In methanol and formamide, the process of establishing the equilibrium position can be captured by the visible absorption spectra. In these two solvents, the IT band absorption is very strong and is the major absorption immediately upon dissolution of the complex. However, over time, as equilibrium is reached, the LMCT band of ferricyanide becomes the major absorption band (Fig. 5). In the strongest electron-accepting solvent, water, little or no decomposition occurs, and the absorption observed is solely due to the intervalence charge transfer.

3.2. Temperature-dependent electrochemistry

Cyclic voltammetric analysis was performed on both **A** and **B**; the results are summarized in Table 2. A linear dependence of peak current with the square root of the scan rate is observed between 5 mV s^{-1} and 1 V s^{-1} (the highest rate employed) indicative of a diffusion limited process. The cyclic voltammograms show a single set of waves corresponding to the electrochemical reaction expressed by the following equation.

$$Fe^{III}/Pt^{IV}/Fe^{III} + 2e^- \rightleftharpoons Fe^{II}/Pt^{IV}/Fe^{II} \quad (4)$$

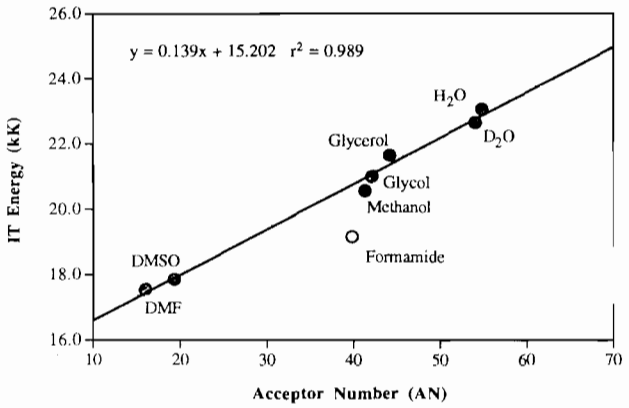

Fig. 4. Plot of IT energy of complex **B** vs. acceptor number of solvents.

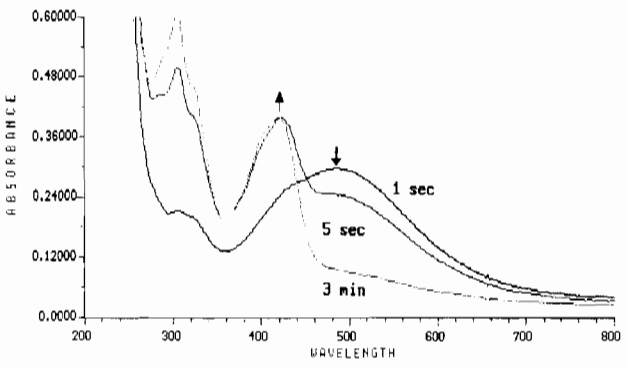

Fig. 5. Absorption spectrum of complex **B** at different time intervals after dissolution in methanol.

Table 2
Electrochemical and photochemical properties of complexes **A** and **B**

	Complex **A**	Complex **B**
Abs. λ_{max} (nm)	424	434
Molar absorptivity (M^{-1} cm^{-1})	2600	2100
$E_{1/2}$ (V vs. SCE)	0.54	0.56
Rate constant[a] (s^{-1} M^{-1})	0.0077	0.39
Stability constant	10^6	7.3×10^8
Quantum yield[b]	0.01	0.015
Entropy[c] (J mol^{-1} K^{-1})	−111	−99.3
Enthalpy[c] (kJ mol^{-1})	170	165

[a]Rate constant is for the redox reaction of $K_3Fe(CN)_6$ and the Pt(II) complex, which is first-order in each of the reactants.
[b]Quantum yield of photodissociation, calculated in terms of the product ferricyanide.
[c]For the redox reaction of Fe centers in the complexes.

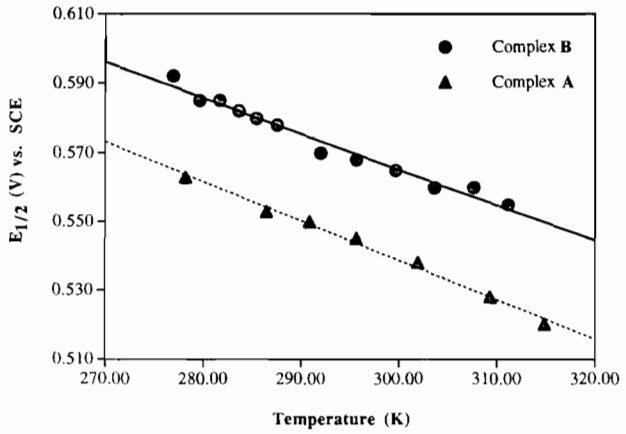

Fig. 6. Plot of temperature dependent redox potential ($E_{1/2}$) for complexes **A** and **B**. Entropy of reduction was calculated from the slope of the line.

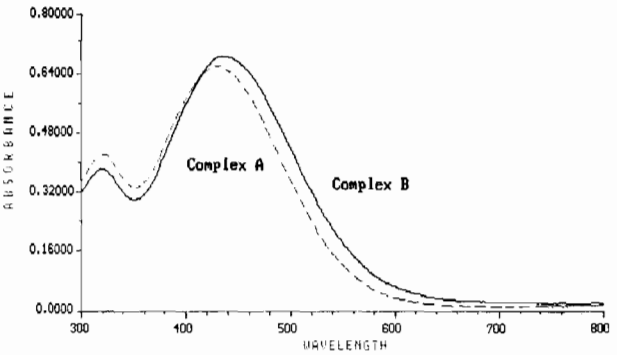

Fig. 7. UV–Vis absorption spectra of complexes **A** and **B**.

The single redox process shows that there is no electronic coupling between the two Fe centers. Reversible two-electron redox behavior was observed in both cases with similar half wave potentials [3]. This is to be expected, considering the fact that the observed redox wave corresponds to the reaction of the $[Fe(CN)_6]^{4-/3-}$ fragments, which are in the same environment in both complexes. The $Pt^{IV/II}$ moiety is electrochemically inactive for kinetic reasons, however, its redox potential can be obtained indirectly by a previously described titration method [4] using DMSO to shift the redox potential of the Fe centers in the complex. When the redox potential of the Fe centers is shifted to a point nearly identical to that of the Pt center, the complex undergoes the decomposition characterized by Eq. (3). This can be monitored by observing the intensity of the IT band in the absorption spectrum. At the critical DMSO mole fraction, the measured redox potential of $[Fe(CN)_6]^{4-/3-}$ moiety is the same as the redox potential for the $Pt^{IV/II}$ couple. This value is 0.40 V versus SCE for **A** and 0.44 V versus SCE for **B**. The small difference in Pt redox potential can be explained by the slightly different electronic structure of the ligands about the Pt site. The ethylene unit of en is more electron-withdrawing than the amine protons, thereby stabilizing the lower oxidation state, Pt^{II}, and shifting the redox potential more positive.

The temperature dependence of redox potential was investigated over the temperature range 3–45 °C (the complexes decompose at higher temperatures). A plot of $E_{1/2}$ for $Fe^{III/II}$ versus temperature was found to be linear as shown in Fig. 6. On the other hand, the redox potential of the $Pt^{IV/II}$ couple was found to be relatively constant in the temperature range investigated.

Since these trinuclear complexes have been classified as essentially valence localized [4]; the total reaction entropy can be considered as a sum of the entropy changes arising from each of the metal centers. Yee et al. [12] have shown that the temperature dependence for individual redox potentials can be identified with good accuracy with true half-reaction entropies. Therefore, the reaction entropy can be obtained from the slope of the lines in Fig. 6, that is, $\Delta S = dE_{1/2}/dT$ yielding -111 ± 4.2 J mol^{-1} K^{-1} for **A** and -99.3 ± 4.9 J mol^{-1} K^{-1} for **B**. Since no measurable temperature dependence was observed for the $Pt^{IV/II}$ couple, the measured reaction entropy is simply the reaction entropy of the ferri/ferrocyanide couple. These values may be compared with the literature values of -96.3 ± 5.9 J mol^{-1} K^{-1} for $[Fe(CN)_6]^{3-/4-}$ bridged to the Ru^{3+} ion [13] through –CN, and -96.3 J mol^{-1} K^{-1} for $[Fe(CN)_6]^{3-/4-}$ ion-paired to the La^{3+} ion [14].

3.3. Temperature-dependent IT band energy

The electronic transition spectra of the complexes are shown in Fig. 7. In each case a broad band tailing well into the red is present, and is assigned to a metal-to-metal intervalence charge transfer (IT) transition as indicated in Eq. (5).

$$Fe^{II}/Pt^{IV}/Fe^{II} \xrightarrow{h\nu} [Fe^{III}/Pt^{III}/Fe^{II}]^* \quad (5)$$

The absorption maximum is 424 and 434 nm for complex **A** and **B**, respectively, consistent with the electrochemical results. The charge transfer theories of Marcus [15,16] and Hush [17] are expected to correlate the optical charge transfer energy (E_{op}) and redox potential in the molecules of interest. In this context, E_{op} is equated with $\lambda + \Delta E$, where λ is the reorganization energy and ΔE is the difference in redox potentials of the metal centers. The more positive $E_{1/2}$ value of $[Pt(en)_2]^{2+/4+}$ compared to $[Pt(NH_3)_4]^{2+/4+}$ gives a smaller difference in redox potentials, and thus a lower energy for the IT band.

The temperature dependence of redox potential discussed previously inevitably leads to a temperature dependence of IT band energy. The absorption maximum of each complex was recorded over the same temperature range used for the electrochemical studies (Fig. 8). As the temperature increases, the absorption maximum red shifts by 17.3 ± 1.1 cm^{-1}/K (-206 ± 14 J mol^{-1} K^{-1}) for complex **A** and 14.4 ± 0.7 cm^{-1}/K (-172 ± 8.1 J mol^{-1} K^{-1}) for complex **B**.

Hush's treatment of optically induced electron transfer energies can be stated as:

$$E_{op} = \lambda_{vib} + \lambda_s + \Delta E \quad (6)$$

where λ_{vib} and λ_s are the molecular vibrational reorganization energy and solvent reorganization energies, respectively, and ΔE is the energy difference between the vibrationally relaxed initial (Pt^{IV} species) and final states (Pt^{III} species). Although all these terms are written in internal energies, Marcus and Sutin [18] argued that they are better viewed as free energies. In this case, the observed temperature dependence can be equated to the entropy of reaction. Thus, the entropy contributions from the vibrational reorganization, solvent reorganization and redox asymmetry is ultimately responsible for the observed temperature dependence of the optical IT transition energy. From this, it follows that:

$$\frac{dE_{op}}{dT} = \Delta S_{rxn} = \frac{d\lambda_{vib}}{dT} + \frac{d\lambda_s}{dT} + \frac{d\Delta E}{dT} \quad (7)$$

However, it has been argued by Hupp [10,19] that the overall temperature dependence of the vibrational reorganization and solvent reorganization energies in water are small. Therefore,

$$\Delta S_{rxn} \approx \Delta S(Pt^{IV/III}) - \Delta S(Fe^{III/II}) \quad (8)$$

The entropy change for the one-electron reduction of platinum can be estimated when the other components of the equation are known. Using the experimental value of $\Delta S(Fe^{III/II}) = -111 \pm 4.2$ J mol^{-1} K^{-1} and $\Delta S_{rxn} = -205 \pm 14$ J mol^{-1} K^{-1} for complex **A** yields $\Delta S(Pt^{IV/III}) = -317 \pm 14.6$ J mol^{-1} K^{-1}. A similar calculation was performed for **B**, giving $\Delta S(Pt^{IV/III}) = -271.3 \pm 9.5$ J mol^{-1} K^{-1}. The large negative values of entropy change associated with the redox reaction of the Pt center indicate that the formation of the Pt^{III} species is entropically unfavored.

3.4. Solvent gated photochemistry

We previously reported [4] that the optically induced charge transfer results in the photodissociation of the trinuclear complex in aqueous solution via cleavage of the cyanide N to Pt bonds. Recent experiments have shown that the presence of DMSO in the aqueous solution changes the IT energy, and subsequently alters the quantum yield of photodissociation.

A general trend of increasing quantum yield with increasing DMSO mole fraction was observed (Fig. 9). This trend can be quantitatively explained by the relatively poor electron-accepting ability of DMSO. It does not accept electron density from the cyanide ligands as well as water (which does so via a hydrogen bonding interaction), therefore, raising the ground state energy

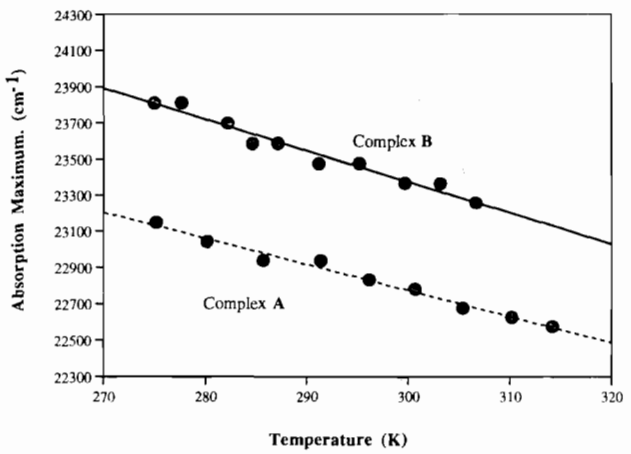

Fig. 8. Plot of temperature dependent IT band energy (i.e., absorption maximum) for complexes **A** and **B**.

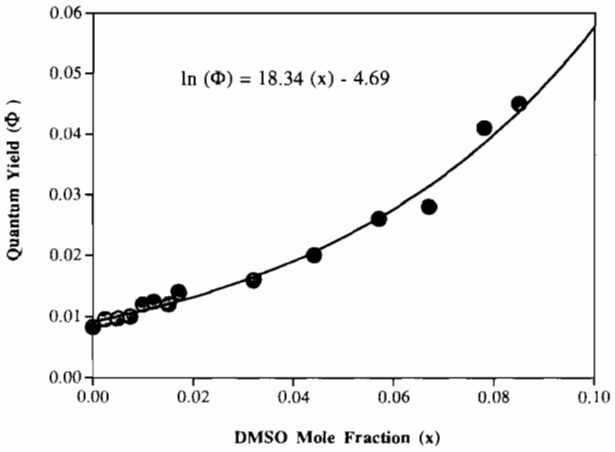

Fig. 9. Plot of quantum yield as a function of DMSO mole fractions for complex **A**.

of $[Fe(CN)_6]^{4-}$. Consequently, the iron units become easier to oxidize, leading to a higher quantum yield.

To investigate the quantitative relationship between the quantum yield and the DMSO mole fraction, the effect of DMSO on the redox potential of ferri/ferrocyanide unit must first be assessed. A plot depicting the linear relationship between $E_{1/2}$ and the DMSO mole fraction is shown in the inset of Fig. 10. Since the Pt redox potential is solvent independent in this system, $\Delta E_R{}^0$, the difference between the Fe and Pt redox potentials, is also linear with respect to the DMSO mole fraction. The model outlined in Fig. 1 suggests that the mole fraction of DMSO should control the observed quantum yield (Φ_{obs}) by shifting $\Delta E_R{}^0$. Experimentally, a logarithmic relationship is observed between Φ and $\Delta E_R{}^0$, as shown in Fig. 10. This observation can be quantitated using the Marcus–Hush model. Within the context of this model, the net two electron process can be expressed by the equations provided in Scheme 1 which utilizes the lettering in Fig. 1.

$$A \overset{h\nu}{\rightleftharpoons} F$$
$$F \xrightarrow[k_{21}]{} C$$
$$C \xrightarrow[k_{23}]{} A$$
$$C \longrightarrow E$$

Scheme 1.

Referring to Scheme 1 it can be seen that the overall or observed quantum yield can be taken as the product of the quantum yields corresponding to the two consecutive one-electron transfer steps. If the quantum yield of reaching the intermediate C is defined as Φ_1 and the quantum yield from intermediate C to product E is defined as Φ_2, then the following equations can be written:

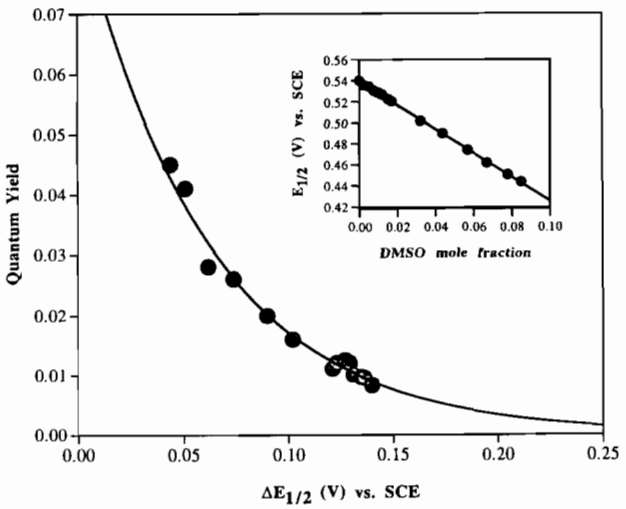

Fig. 10. Quantum yield vs. $\Delta E_R{}^0$ for complex **A**. The inset included is a plot of redox potential at different DMSO mole fractions.

$$\Phi_{obs} = \Phi_1 \times \Phi_2 \tag{9}$$

$$\Phi_2 = \frac{k_{23}}{k_{23}+k_{21}} \tag{10}$$

The reaction rates k_{23} and k_{21} are the thermal rate constants of C→E and C→A, respectively. They can be further substituted by the activation energy of the two pathways assuming that Arrhenius type behavior holds:

$$k_{23} = A \exp(-E_{a23}/RT) \tag{11a}$$

$$k_{21} = A' \exp(-E_{a21}/RT) \tag{11b}$$

Taking the reciprocal of (9) and substituting Eqs. (10) and (11), one obtains:

$$\frac{1}{\Phi_{obs}} = \frac{1}{\Phi_1}\frac{A}{A'}\exp\left(\frac{E_{a23}-E_{a23}}{RT}\right) + \frac{1}{\Phi_1} \tag{12}$$

From the potential surface in Fig. 1, it can be seen that

$$E_{a21} = E_{th32} - \Delta E_{23} \tag{13a}$$

$$E_{a23} = E_{th12} - \Delta E_{12} \tag{13b}$$

$$\Delta E_{13} = \Delta E_{12} - \Delta E_{23} \tag{13c}$$

Substituting these relations into Eq. (12), one obtains the following

$$\frac{1}{\Phi_{obs}} = \frac{1}{\Phi_1}\frac{A}{A'}\exp\left(\frac{E_{th32}-E_{th12}+\Delta E_{13}}{RT}\right) + \frac{1}{\Phi_1} \tag{14}$$

in which $1/\Phi_{obs}$, E_{th32}, E_{th12} and ΔE_{13} can all be measured.

E_{th32} is the thermal activation energy of forming the Pt(III) species from $Fe(CN)_6{}^{3-}$ and $Pt(NH_3)_4{}^{2+}$. Since this step is the rate determining step in the formation of the trinuclear complex, its activation energy can be calculated from the reaction rates of formation. E_{th12} is the thermal activation energy of intervalence charge transfer of the trinuclear complex. According to Hush's theory, E_{th12} can be obtained from the IT band energy (E_{op}):

$$E_{th12} = E_{op}{}^2/4\lambda \tag{15}$$

In addition, $\lambda = E_{op} - \Delta E_{12}$, where ΔE_{12} is the ground state energy difference between the Pt(IV) species and the intermediate Pt(III) species, i.e.

$$\Delta E_{12} = E_{1/2}(Fe^{2+/3+}) - E_{1/2}(Pt^{3+/4+}) \tag{16}$$

The redox potential of the $Pt^{3+/4+}$ couple has been estimated to be −0.56 V versus SCE [4], and is assumed to be constant regardless of the DMSO mole fraction. The redox potential of the $Fe^{2+/3+}$ couple was measured by cyclic voltammetry in appropriate solvent mixtures. E_{op} was directly obtained from absorption measurements with the added assumption that the IT band energy shifts linearly with the DMSO mole fraction, by the

same magnitude that the redox potential of **A** shifts with the DMSO mole fraction. The IT band was found to move from 424 to 560 nm as the DMSO mole fraction was increased from 0 to 0.34, beyond which there was virtually no IT band to observe due to the decomposition of the complex via Eq. (3).

ΔE_{13} is the ground state energy difference between parabolas 1 and 3 (Fig. 1). Obviously,

$$\Delta E_{13} = E_{1/2}(Fe^{3+/2+}) - E_{1/2}(Pt^{4+/2+}) \quad (17)$$

Having established all the above parameters at respective DMSO mole fractions, a plot of $1/\Phi_{obs}$ versus the exponential term in Eq. (14) can be generated, and it should give a straight line. This linear relationship was indeed observed as shown in Fig. 11. A curve fit of the data shows that the slope is equal to 158 ± 20 and the y-intercept is 11.4 ± 7.7. From these values, Φ_1 and the ratio A/A' were calculated to be 0.088 and 13.8, respectively. The small value of Φ_1 indicates that the majority of the excited state complex generated upon light absorption quickly relaxes to the ground state reactant through a non-radiative pathway; only a small fraction ($\sim 9\%$) reaches the intermediate $Fe^{III}/Pt^{III}/Fe^{II}$. This is consistent with that fact mentioned previously that the formation of the Pt^{III} species is entropically unfavored.

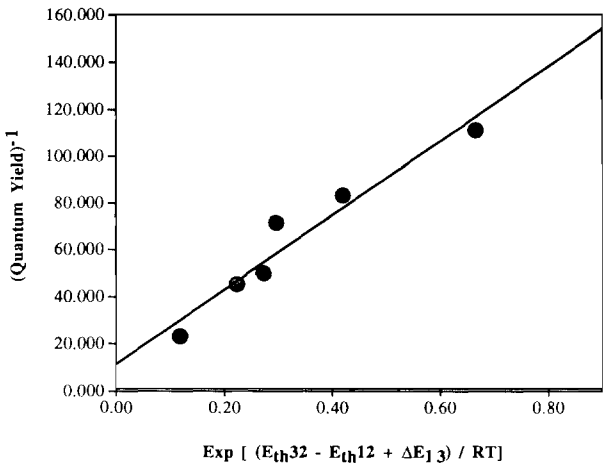

Fig. 11. Plot of reciprocal quantum yield as a function of activation energies for complex **A**.

4. Conclusions

In summary, we have demonstrated that the Marcus–Hush theory, which has been successfully applied to many binuclear mixed-valent complexes, is also valid for trinuclear mixed-valent complexes involving not just one, but two-electron transfer processes. The temperature- and solvent-dependent intervalence charge transfer can both be interpreted in terms of the shift in the free energy of the charge transfer reaction of the metal centers involved. The two phenomena are related.

Acknowledgement

The United States National Science Foundation is thanked for support of this work under Grant No. CHE-9312056.

References

[1] L.A. Worl, G.F. Strouse, J.N. Younathan, S.M. Baxter and T.J. Meyer, *J. Am. Chem. Soc., 112* (1990) 7571–7578, and refs. therein.
[2] B.W. Pfennig and A.B. Bocarsly, *Comments Inorg. Chem., 13* (1992) 261–275.
[3] M. Zhou, B.W. Pfennig, J. Steiger, D. Van Engen and A.B. Bocarsly, *Inorg. Chem., 29* (1990) 2457–2460.
[4] B.W. Pfennig and A.B. Bocarsly, *J. Phys. Chem., 96* (1992) 226–233.
[5] A.B. Pfennig and A.B. Bocarsly, *Coord. Chem. Rev., 111* (1991) 91–96.
[6] W.C. Vosburgh and G.R. Cooper, *J. Am. Chem. Soc., 63* (1941) 437.
[7] U. Mayer, V. Gutmann and W. Gerger, *Monatsh. Chem., 106* (1975) 1235–1257.
[8] C. Reichardt, *Solvents and Solvent Effects in Organic Chemistry*, VCH, Weinheim, Germany, 2nd edn., 1988.
[9] H.Z. Kriegsmann, *Z. Phys. Chem. (Leipzig), 269* (1988) 1030–1036.
[10] V. Gutmann, *The Donor–Acceptor Approach to Molecular Interactions*, Plenum, New York, 1978.
[11] V. Gutmann, *Electrochim. Acta, 21* (1976) 661–670.
[12] E.L. Yee, R.J. Cave, K.L. Guyer, P.D. Tyama and M.J. Weaver, *J. Am. Chem. Soc., 101* (1979) 1131.
[13] Y. Dong and J.T. Hupp, *Inorg. Chem., 31* (1992) 3322–3324.
[14] J.T. Hupp and M.J. Weaver, *Inorg. Chem., 23* (1984) 256.
[15] R.A. Marcus, *J. Chem. Phys., 24* (1956) 966.
[16] R.A. Marcus, *J. Chem. Phys., 43* (1965) 679–701.
[17] N.S. Hush, *Prog. Inorg. Chem., 8* (1957) 391.
[18] R.A. Marcus and N.S. Sutin, *Comments Inorg. Chem., 5* (1986) 119.
[19] J.T. Hupp and M.J. Weaver, *J. Phys. Chem., 88* (1984) 1860.